CrystEngComm

PAPER

View Article Online
View Journal | View Issue

Cite this: *CrystEngComm*, 2023, **25**, 2591

In situ Raman study of the crystallization of glycine†

Jingjing Wang, [a] Adriana Alieva,[a] Matthew Boyes, [a] Andrew J. Pollard [b] and Cinzia Casiraghi *[a]

The process of crystallization of organic molecules is a well-known effect. However, a full understanding of this process is still lacking because it is very challenging to monitor fast changes in the molecular interactions. In this work, we perform an *in situ* study on the crystallization of glycine upon H_2O and D_2O evaporation by micro-Raman spectroscopy. The magnitude of the frequency splitting between the high-frequency asymmetric and the low-frequency symmetric CH_2 stretching components is used to determine the dihedral angle ξ, which measures the deviation from the planar glycine conformation through rotation around the C–C bond, hence providing insights on the molecular arrangement. Our results show that the average ξ of the glycine molecules in both H_2O and D_2O is ~20°, and it does decrease to ~18° when the mature crystal is formed, corresponding to the molecular arrangement of α-glycine. However, right before the crystal is fully formed, a complex CH peak lineshape is observed, indicating that some of the molecules have ξ ~22°, which is close to the molecular arrangement of β-glycine. Our results show that glycine molecules in water do not crystallize directly into a perfect α-glycine crystal, but a metastable state is first formed, where some of the molecules are more bent as compared to the α-glycine configuration.

Received 13th March 2023,
Accepted 28th March 2023

DOI: 10.1039/d3ce00241a

rsc.li/crystengcomm

Introduction

Crystallization from solution is a well-known phenomenon that has been observed since the early centuries, and it is exploited by a wide range of industries.[1] However, the production of organic crystals with specific properties, such as crystal size, shape, and polymorph is still very difficult because getting insight on the dynamics of the crystallization process is itself very challenging – it often occurs at a broad range of length and exceedingly small time scales.[2–5] Several experimental techniques[6] and computational methodologies[3] have been used to study the dynamics of the crystallization process from solution, such as cryo- and liquid-phase transmission electron microscopy.[6–9] Despite the high spatial resolution of electron microscope based techniques, this approach is very time consuming and requires specific sample preparation. Moreover, the temporal resolution of the measurement is only maintained in the order of seconds.[3,10] Electrospray ionization mass spectrometry and analytical ultracentrifugation analysis have also been used to study the formation of pre-nucleation clusters.[11,12] Both methods are capable of monitoring the entirety of the crystallization process, but they are not sensitive enough to detect the small number of molecules participating in the nucleation process, therefore it is difficult to establish a nanoscopic picture of the crystallization process. Other techniques such as nuclear magnetic resonance,[13,14] X-ray photoelectron spectroscopy,[15,16] and neutron scattering[17] need to be combined with computational modelling studies in order to gain more detailed information on the solute–solvent and solvent–solvent interactions. Amongst all possible characterization techniques, Raman spectroscopy is a simple and fast technique, which is widely used both in crystallization studies,[18,19] and material science,[20,21] and it can be easily implemented in an industrial production line,[22] In particular, recent studies[23,24] have used *in situ* Raman spectroscopy to study the crystal nucleation of glycine with the aim of identifying the nature of the intermediate clusters and their transformation to the final crystalline form. These works claim that Raman spectroscopy is able to identify the nature of the intermediate state during nucleation: Liao and Wynne observed an amorphous intermediate and indicated that the nucleation process takes place through a number of intermediate stages, finally resulting in the formation of one of the crystal polymorphs.[23] Urquidi *et al.* proposed that the structure of glycine pre-nucleation aggregates may be hydrogen-bonded linear networks.[24] However, some

[a] *Department of Chemistry, University of Manchester, Manchester, M13 9PL, UK. E-mail: cinzia.casiraghi@manchester.ac.uk*
[b] *National Physical Laboratory, Teddington, Middlesex, TW11 0LW, UK*

† Electronic supplementary information (ESI) available: It contains details on the crystallization setup and additional Raman measurements and related fits of the CH peaks. See DOI: https://doi.org/10.1039/d3ce00241a

controversies did arise related to the use of optical trapping in this work, which may be likely to attract amorphous aggregates present in solution, rather than states associated with the nucleation process.[25,26] Therefore, the potential of Raman spectroscopy in studying the processes associated to nucleation and crystallization is still not completely clear.

In this work we perform *in situ* micro-Raman spectroscopy on an evaporating micro-droplet of aqueous glycine solution, deposited on a silicon (Si/SiO_2) substrate, enabling us to perform non-invasive measurements on a very small volume of liquid to avoid effects caused by foreign surfaces in contact with the solution. A microscope-based setup is used in order to focus the laser beam inside the droplet, hence achieving high sensitivity, in contrast to the traditional setup based on the use of optical fibers.[27] Note that evaporating droplets are commonly used to study crystallization because they offer a simple and well defined system that can be easily applied in many applications, from ink-jet printing,[28,29] and spray coating[30] to pharmaceuticals[31] and environmental science.[32]

Glycine has been selected for this study because its polymorphism is well studied.[31] In contrast to previous works, we exploit the fact the Raman spectroscopy is extremely sensitive to the molecular packing, including small structural alterations such as bond lengths, dihedral angles, and hydrogen bonding patterns.[33] In particular, it has been shown that the positions of the two CH stretching vibrations not only allow for the identification of the glycine polymorph,[34] but can also be used to identify the dihedral angle ξ, defined by atoms N–C–C–O_{cis} to N, Fig. 1a, hence providing direct information on the molecular arrangement. By fitting the CH stretching peaks and determining how their splitting difference changes during the evaporation of the solvent, we observed that there is a sharp transition in the molecular arrangement from solvated molecules to glycine crystals, with the final polymorph being α-glycine ($\xi \sim 18°$), in agreement with previous results.[35] However, right before the mature α-glycine is observed, the CH doublet of glycine shows a complex shape, indicating the presence of two molecular arrangements, one corresponding to $\xi \sim 18°$, and another associated to $\xi \sim 22°$. This second component quickly disappears as soon as crystal growth takes place, leading to the final α-glycine crystal, where all molecules have $\xi \sim 18°$. The same result is obtained regardless if the measurements are performed close to the edge of the droplet, where nucleation is preferred, or in the centre of the droplet, associated to preferential crystal growth. Therefore, this shows that the mixed arrangement we have observed cannot be associated to the nucleation processes, but it must be related to crystal growth, *i.e.* glycine molecules in water do not crystallize directly into a perfect α-glycine crystal, but a

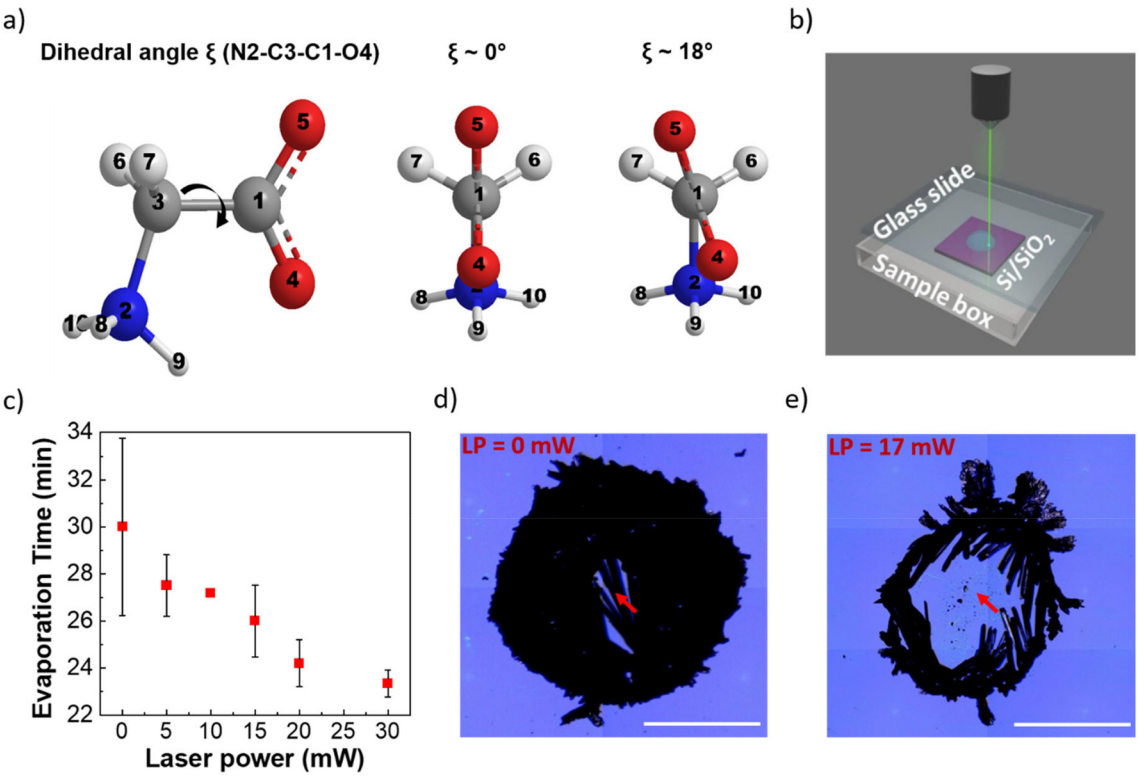

Fig. 1 a) Schematic of the structure of glycine, showing the dihedral angle and example of two configurations. At $\xi = 0°$, the molecule is planar since the C–H bonds are symmetrically disposed on the COO plane, while at $\xi = 18°$, the C–H bonds are asymmetrical since they are disposed on both sides of the COO plane (adapted from ref. 33). b) Schematic of the experimental set-up. c) Evaporation time measured by exposing the solution to a laser beam with increasing power (LP). Optical images of glycine crystals obtained: d) without exposing the laser (LP = 0 mW) and: e) by exposing the solution with LP = 17 mW. Scale bars ~0.5 mm. The laser beam position was in the centre of the droplet in both cases, as indicated by the red arrow.

metastable state is first formed, in agreement with results obtained with other techniques.[36]

In conclusion, we show that micro-Raman spectroscopy, without use of optical trapping, is able to provide important information on the changes in the molecular arrangement during liquid to solid transition and to provide information on the crystal growth.

Methods

Materials

Glycine powder (Reagent Plus ≥99%), isopropanol (IPA, ≥95%), acetone, and D_2O (99.9 atom% D) were purchased from Sigma-Aldrich. Type 1 de-ionised (DI) water was dispensed from a Millipore Direct-Q® 3UV water purification system with a resistivity of 18.2 MΩ cm at room temperature. Silicon wafers with an oxide layer thickness of 290 nm were purchased from Inseto Ltd (UK) and they were cleaned with acetone and then IPA in an ultrasonic bath for 15 minutes prior to any use and dried by N_2 flow. Plastic sample boxes with dimensions of 25 mm × 25 mm × 8 mm were purchased from Agar Scientific.

Crystallization setup

A 0.5 M of an undersaturated aqueous glycine solution was prepared by dissolving glycine in either DI water or D_2O by stirring at 50 °C for 1 hour. A clean silicon substrate was placed in a plastic box and 2 μL of the glycine solution was drop-cast using a micropipette onto the Si/SiO_2 substrate. The box was partially covered with a glass cover slide leaving ~1 mm gap, Fig. 1b and S1,† to slow down the evaporation rate in order to allow sufficient time to collect several Raman spectra over the crystallization process. More information on the setup is available in section S1 in the ESI.†

In situ Raman spectroscopy

All measurements were performed with a Renishaw inVia™ Reflex Raman spectrometer equipped with a laser with an excitation wavelength of 514.5 nm. The measurements were taken with a 100X long distance objective (NA = 0.6), giving a laser spot size of ~800 nm, and using ~10 mW laser power. The fingerprint (FP) region between 500 and 1700 cm^{-1} and CH stretching region between 2850 and 3100 cm^{-1} were measured separately with an 1800 grooves per mm and 2400 grooves per mm grating, respectively. The measurements are taken after a few minutes from deposition of the droplets on the substrate (taken as time = 0) until crystallization is complete, *i.e.* when the crystals are seen by eyes. As the laser is focussed through an objective, it is possible to carefully select where to take the measurements with respect to the droplet shape. This is very important because the crystals are known to nucleate from the edge of the droplet and then to growth towards the centre.[37–39] Hence, two set of measurements were taken: one close to the edge of the droplet (~700 μm from the centre of the droplet) and another exactly in the centre (see section S2.1 in the ESI† for more details).

Because the Raman intensities of the FP and CH modes are different, measurements were taken under different conditions to enable a good signal-to-noise ratio: in the case of glycine solutions in H_2O, the FP region measurements were taken every 60 s (*i.e.* one spectrum measurement takes 60 s) for 24 minutes, after which the acquisition time was reduced to 30 s until no further changes in the spectrum were observed. For the CH region, measurements were taken every 90 s for 16.5 minutes, then the acquisition time was reduced to 60 s until 24.5 minutes. After this, spectra were collected every 30 s until no further change was observed. For the measurements in D_2O, the FP region spectra were collected every 90 s for 17 minutes, then every 60 s for the next 11 minutes, and finally every 30 s until no further change was detected. For the CH region, the measurements were taken every 90 s for 16.5 minutes, then every 60 s for the next 8 minutes, and finally every 30 s until no further change was observed. Both measurements in H_2O and D_2O were repeated 10 times, using fresh solution for each experiment in order to ensure the reliability of the collect results and rule out effects from impurities. The different measurements time in D_2O and H_2O are due to the different evaporation time of the two solvents (section S1, ESI†).

The CH peaks were fitted with Lorentzian functions. The position and the full width at half maximum (FWHM) were tabulated from the fits.

We focus our analysis on the high-frequency asymmetric and the low-frequency symmetric CH_2 stretching components, $\nu_{as}(CH)$ and $\nu_s(CH_2)$, respectively. The magnitude of the frequency splitting between the $\nu_s(CH)$ and $\nu_{as}(CH)$ modes, Δ_{CH}, gives insights into the conformation of the glycine molecules, given by the dihedral angle ξ, Fig. 1a, which indicates the deviation of glycine crystal from the planar conformation through rotation around the C–C bond. Fig. 1a shows two glycine molecules corresponding to $\xi = 0°$ (*i.e.* all heavy atoms in the glycine molecule lie in the same plane) and $\xi = 18°$, which is the molecular arrangement in the α-glycine crystal. Note that the in the β-glycine ξ is ~22°. Although the difference in angle is small, the corresponding CH splitting can be resolved by Raman spectroscopy, hence enabling this technique to be used for polymorph screening.

Results

Optimization of the laser power (LP)

It is well known that performing Raman spectroscopy with a confocal microscope enables to concentrate the laser power into a relatively small area, hence achieving a high signal from a well-defined and small region (comparable to the laser spot size) of the sample. On the other side, if the power is too high, a strong increase in the local temperature of the sample could occur, which in our specific case will affect the evaporation rate and the crystallization outcome.[40,41] In this study, we want to minimize any effect on crystallization from

exposure of the solution to the laser beam, but at the same time we need to have enough laser power to resolve the Raman peaks from the background noise. To optimize the experimental setup, first we performed crystallization experiments by exposing the solution to increasing laser power, ranging from 0 mW to 20 mW and by focussing the laser exactly in the centre of the droplet. The evaporation time of three evaporations of aqueous glycine solution exposed to different laser powers were compared with the evaporation time of the control samples (*i.e.* no laser exposure), calculated from the average of 10 crystallisation experiments. Fig. 1c shows that an increase of laser power leads to faster evaporation. The laser power also affects the morphology of the crystals. Comparing the representative optical images of Fig. 1d and e, one can see that the use of high laser power makes the crystals to preferentially grow around the edge of the droplet, avoiding the centre where the laser beam has been focused. This effect is due to the temperature gradient produced inside the droplet, forcing a greater mass transport of glycine molecules to the edge. To minimize any effect from the laser heating and allow for acceptable data acquisition, we performed measurements at a fixed power of 10 mW.

Raman measurements at the edge of the droplet

Glycine crystallization in H_2O

Fig. 2a illustrates the evolution of the Raman spectrum of the FP region over time. For the sake of simplicity, we focus our analysis on the three most prominent peaks: the ν(C–C) & ν(C–N), $\tau(CH_2)$, and $\nu_s(CO_2)$, located at ~898 cm^{-1}, 1330 cm^{-1} and 1411 cm^{-1}, respectively.[42] The evolution of their positions and FWHM during solvent evaporation is shown in Fig. 2b and c, respectively.

Fig. 2 shows that there is a sharp decrease in the peaks position and FWHM after about 21 min, associated to the phase change from liquid to solid. After 23 minutes the crystals are formed, as confirmed by the disappearance of the second order silicon peak at ~1000 cm^{-1}, *i.e.* the crystals are now so large that the laser cannot reach the silicon substrate, and by the peak positions, corresponding to those observed in α-glycine.[23,43,44] We also observe the peak at 1450 cm^{-1} to become a doublet in the mature crystal – this has never been observed before, and could be the result of the better spectral resolution of our spectrometer as compared to previous studies.[43] Note that during water evaporation in the first 21 minutes, a small decrease in position and FWHM can be observed, in particular for the $\tau(CH_2)$ peak, where the changes are clearly above the spectral resolution of the spectrometer (1–2 cm^{-1}). This could be a consequence of a decrease in the number of water molecules, due to the solvent evaporation, rather than changes in the interactions between glycine molecules.[42]

Fig. 3a illustrates the evolution of the Raman spectrum of the CH region over time. Fig. 3b and c show the positions and FWHM of the ν_{as}(CH) and ν_s(CH) peaks. Sharp changes in both parameters are observed after 15 minutes, corresponding to the transition from liquid to solid state. Note that the times cannot be compared to the ones in Fig. 2 as the measurements are taken separately, due to the different signal strength of the FP and CH regions. The peak positions of ν_s(CH) and ν_{as}(CH) after 17.5 min do not change further and corresponds to 2971 cm^{-1} and 3007 cm^{-1},

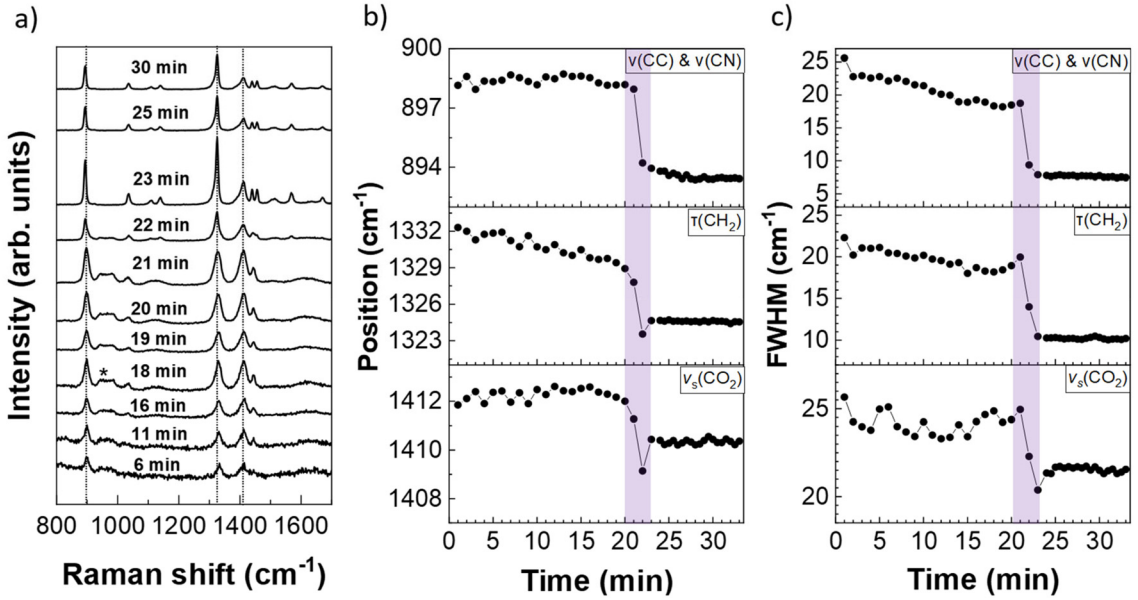

Fig. 2 a) Evolution of the FP region of the Raman spectrum of glycine crystallising from H_2O. b) Peak position and c) FWHM of the ν(C–C) & ν(C–N), $\tau(CH_2)$, and $\nu_s(CO_2)$ modes as a function of the crystallization time. * indicates the silicon peak. The purple shadow shows the transition from liquid to solid state.

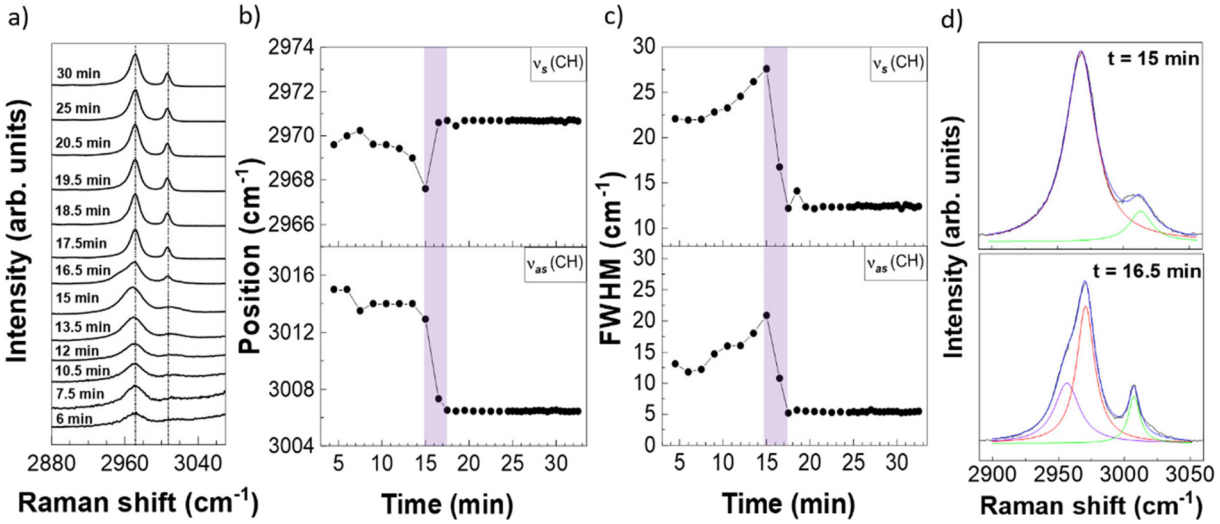

Fig. 3 a) Evolution of the CH region of the Raman spectrum of glycine crystallising from H_2O. b) Peak position and c) FWHM of ν_s(CH) and ν_{as}(CH) as function of the crystallization time. d) Fits of the CH region of the Raman spectrum measured at 15 minutes (top panel) and 16.5 minutes (bottom panel). The purple shadow shows the transition from liquid to solid state.

respectively, indicating that α-glycine is formed,[43] in agreement with the results obtained from the FP region analysis (Fig. 2). One can also observe that solvent evaporation produces a clear increase in the FWHM of both CH stretching modes, in contrast to the FP modes.[23] This suggests that the CH modes are more sensitive to intermolecular interactions as compared to the FP modes.[43]

Fig. 3a also shows that the CH mode associated to the transition from liquid to solid, measured at 16.5 min, has a complex lineshape, which is not observed either in the liquid or final crystal forms. Fig. 3d shows the fit of CH peaks measured at 15 and 16.5 min: an additional ν_s(CH) peak located at ~2957 cm^{-1} is clearly seen in the spectrum at 16.5 min, indicating the presence of a mixed molecular arrangement.

Glycine crystallization in D_2O

To investigate any possible effect on the Raman spectra due to H-bonding interactions between water and glycine, in particular during the initial stages of evaporation of the solvent, we conducted the same series of experiments by

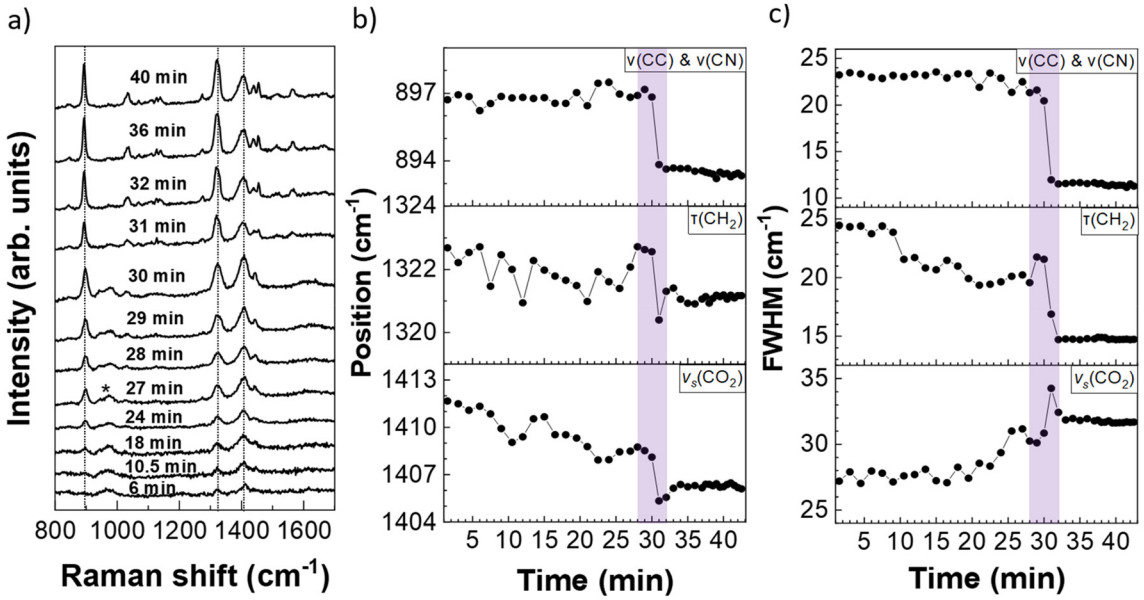

Fig. 4 a) Evolution of the FP region of the Raman spectrum of glycine crystallisation from D_2O. b) Peak position and c) FWHM of the ν(C–C) & ν(C–N), $\tau(CH_2)$, and $\nu_s(CO_2)$ modes with respect to time. * indicates the silicon peak. The purple shadow shows the transition from liquid to solid state.

crystallizing glycine in D_2O. Note that evaporation in D_2O is slower as compared to water, so spectra measured at the same time cannot be compared with the previous ones in H_2O.

Fig. 4a illustrates the evolution of the Raman spectrum of the FP region over time. Fig. 4b and c show the positions and FWHM of the ν(C–C) & ν(C–N), $\tau(CH_2)$, and $\nu_s(CO_2)$, located at ~898 cm^{-1}, 1330 cm^{-1} and 1411 cm^{-1}, respectively, during solvent evaporation. Little change is seen for the first 30 min, till a rapid change in position and FWHM is seen when the final crystalline form is formed at 31 min, corresponding to the formation of α-glycine. This also corresponds to the disappearance of the silicon peak at 1000 cm^{-1}, as observed for the crystallization of glycine from H_2O. The doublet peak at ~1456 cm^{-1} associated to the mature crystals is observed in both crystallizations from H_2O and D_2O (Fig. 2a and 4a). There is also a new peak at 1550 cm^{-1}, corresponding to the asymmetric stretching of carboxyl (COO^-) groups, in agreement with previous works.[40,43]

Remarkably, we observe an increase in the FWHM of the $\nu_s(CO_2)$ band when the experiment is performed in D_2O, in contrast to the results obtained in H_2O (Fig. 2c). This could be due to isotope exchange between the D_2O and the NH_3 group of the glycine molecules, resulting in a deuterated amino group. This exchange is expected to affect the H-bonding network, *i.e.* the H-bonds between the amino group of one glycine molecule and the carboxylate group of its neighbour will be longer. This could distort the crystal unit cell, making it less dense than the protonated form, thereby making it less crystalline. This loss of crystallinity could be the cause of the increase of the FWHM of this particular band – further experiments are needed to confirm this hypothesis.

Fig. 5a illustrates the evolution of the Raman spectrum of the CH region over time. Fig. 5b and c show the positions and FWHM of the ν_{as}(CH) and ν_s(CH) peaks. Sharp changes in both parameters are observed after 28 minutes, corresponding to the transition from liquid to solid state. The peak positions of ν_s(CH) and ν_{as}(CH) after 28.5 min do not change further and correspond to 2971 cm^{-1} and 3007 cm^{-1}, respectively, indicating that α-glycine is formed,[43] in agreement with the results obtained from crystallization in H_2O (Fig. 3). Hence, no difference in the polymorph outcome is observed by changing the solvent.

Fig. 5d shows the spectra measured at the transition region and their corresponding fitting. As in the case of D_2O, an additional peak at 2953 cm^{-1} is observed in the spectrum measured after 27 min, in agreement with the results obtained in H_2O (Fig. 3d).

Note that in the case of D_2O, we could also measure the peak at 2500 cm^{-1}, associated to D–O stretching vibrations, so we can directly detect the presence of the solvent by monitoring this peak. Fig. S2.4 in the ESI† shows that this peak disappear after 27 minutes, hence indicating almost complete solvent evaporation.

Analysis of the dihedral angle

From the fit of the CH stretching peaks (all fits and CH positions are given in section S2 of the ESI†), we found that solvated molecules in H_2O and D_2O have Δ_{CH} of 43–44 cm^{-1}, Fig. 6a. The same shift has been reported by Bykov *et al.* for glycine solution in D_2O.[33] This shift corresponds to ξ ~20°. In the solid phase, Δ_{CH} is ~36 cm^{-1}, Fig. 6a, which corresponds to a dihedral angle of ~15°, in good agreement with the molecular arrangement of α-glycine (ξ ~18°). In the transition phase from liquid to solid, *i.e.* right before the mature crystal is crystallised, an additional ν_s(CH) component is observed at the average position of ~2954 cm^{-1}. The CH positions are tabulated for all experiments in

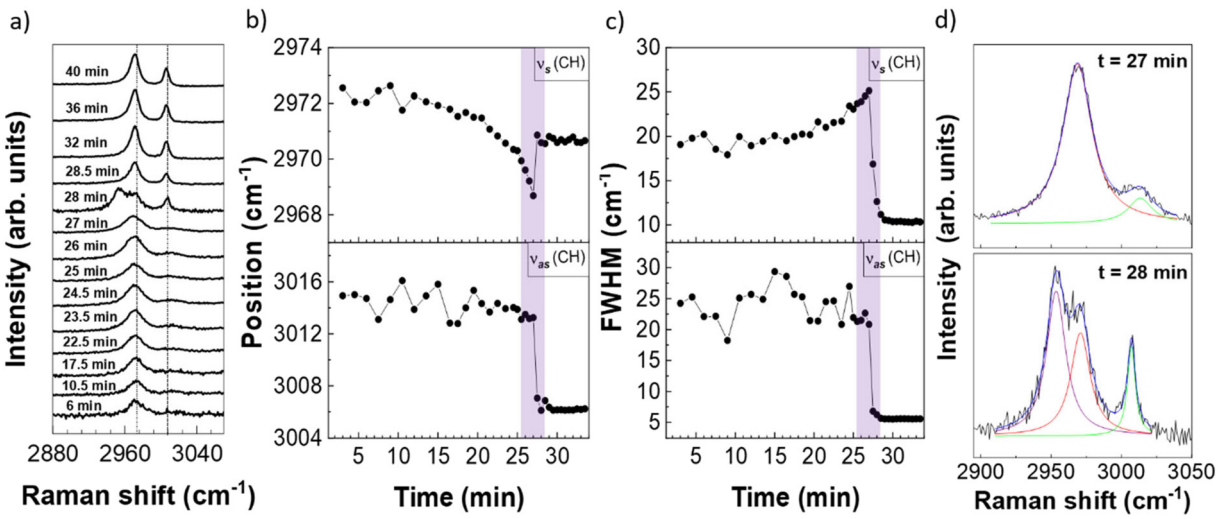

Fig. 5 a) Evolution of the CH region of the Raman spectrum of glycine crystallising from D_2O. b) Peak position and c) FWHM of ν_s(CH) and ν_{as}(CH) as function of the crystallization time. d) Fits of the CH region of the Raman spectrum measured at 27 minutes (top panel) and 28 minutes (bottom panel). The purple shadow shows the transition from liquid to solid state.

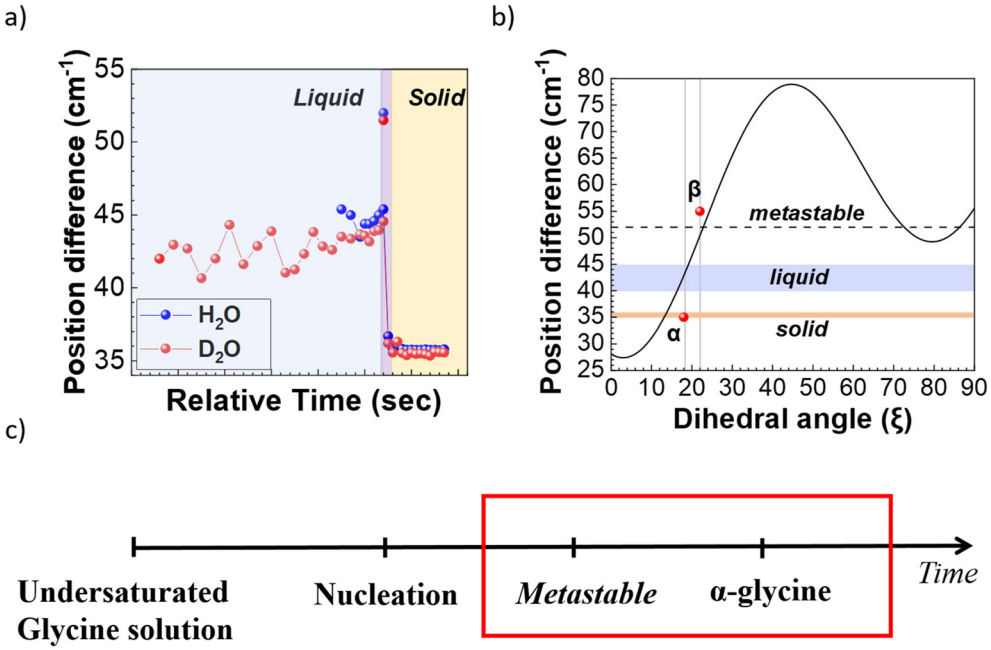

Fig. 6 a) Evolution of the peak position difference of the ν_s(CH) and ν_{as}(CH) modes during crystallisation in H_2O and D_2O. The blue and orange shadows show the glycine molecules in liquid and in solid state, respectively. b) Relation between the splitting frequency of the CH_2 stretching in glycine molecules *versus* the calculated dihedral angles (adapted from ref. 33). c) Schematic of the evolution of the crystallization process. The red box shows when the processes associated to crystal growth – here a change from metastable to stable phase has been observed by *in situ* micro-Raman spectroscopy.

section S2 of the ESI.† As the average ν_{as}(CH) is ~3006 cm^{-1}, this additional component shows Δ_{CH} ~52 cm^{-1}, which corresponds to ξ ~23° (dotted line in Fig. 6b). This splitting is very close to the experimental Δ_{CH} found for β-glycine. It is believed that in homogeneous nucleation experiments at room temperature, the least stable polymorph, β glycine, should nucleate first and then transform into the α or γ polymorph depending on the amount of water present.[40] The nucleation of the β-glycine and subsequent change into the α-glycine has been recently confirmed by nuclear magnetic resonance.[36] Therefore, the additional peak observed in our Raman spectra could be associated to the presence of β-glycine. However, one should note that the FWHM of the additional peak is relatively large (~23 cm^{-1} in both solvents), hence unlikely to be associated to a perfect crystalline phase. Furthermore, the Raman measurements are an average of the different molecular arrangement within the measurement time (few minutes), so our measurements are probing the changes from a metastable phase into the α-glycine. Finally, a Δ_{CH} of 53 cm^{-1} has been calculated for the bent component in triglycine sulphate, where two glycine molecules have geometries close to planar while one glycine molecule is bent.[33]

To conclude, our *in situ* Raman measurements clearly show that the glycine molecules do not crystallize directly into the α-glycine, but a metastable form is nucleated first, where the glycine molecules are more bent as compared to the molecular arrangement observed in the solvated state and in the α-glycine crystal.

Raman measurements at the centre of the droplet

Our results show that Raman spectroscopy can be used to study the changes in the arrangement of the glycine molecules during crystallization from solution. In particular, we observed a mixed arrangement before the mature α-crystal is formed. To identify if this molecular arrangement is related to an intermediate state associated to the process of nucleation or to crystal growth, we performed the same measurements exactly in the centre of the droplet, where nucleation is less likely to happen.[37–39] The crystallization was performed in H_2O. Fig. S2.5† illustrates the evolution of the Raman spectrum of the CH region over time. Fig. S2.6† show representative changes in position and FWHM of the ν_s(CH) and ν_{as}(CH) peaks upon solvent evaporation. Sharp changes in both parameters are observed after 42.5 minutes, corresponding to the transition from liquid to solid state. The peak positions of ν_s(CH) and ν_{as}(CH), corresponding to 2971 cm^{-1} and 3007 cm^{-1} respectively, do not further change after 42.5 minutes. This indicates that the α-glycine is formed,[43] in agreement with the results obtained from crystallization in H_2O at the edge region of the droplet (Fig. 3). Furthermore, the additional ν_s(CH) peak located at 2953 cm^{-1} is clearly seen in all the spectra, giving an average Δ_{CH} of 52 cm^{-1}, in agreement with the measurements performed at the edge region (Fig. 5). Therefore, we can conclude that our Raman measurements do not probe changes in molecular arrangement associated to nucleation, but to crystal growth.

Conclusions

In conclusion, we have studied the crystallisation of glycine in H_2O and D_2O to solid form by *in situ* micro-Raman spectroscopy, using micro-droplet evaporation. During initial evaporation of the solvent, there is a lag time where glycine molecules are surrounded by water molecules and no significant change in the intermolecular vibrations of glycine are observed. The phase change appears as a sharp change in the position and width of the main Raman peaks. By analysing the CH stretching peak positions, we found that, on average, the glycine molecules in both H_2O and D_2O arrange in a configuration associated to a dihedral angle of ~15°, and do crystallize into α-glycine (dihedral angle of ~18°). However, we observe that glycine molecules in water do not crystallize directly into a α-glycine crystal, but a metastable state is first formed, where some of the molecules show a dihedral angle of ~22°, close to the one observed in β-glycine.

Author contributions

J. W. and A. A. performed the crystallization and Raman measurements, J. W. and M. B. analyzed the data obtained; J. W. prepared the initial manuscript. C. C. developed the project and supervised the research with A. J. P. All authors assisted in the writing of the final manuscript.

Conflicts of interest

There are no conflicts to declare.

Acknowledgements

This work is supported by the European Research Council (ERC) under the European Union's Horizon 2020 research and innovation programme under grant agreement No 648417. The authors thank Katharina Edkins for useful discussions.

References

1 J. Bernstein, *Polymorphism in Molecular Crystals*, Oxford University Press, New York, 2010.
2 M. J. Van Vleet, T. Weng, X. Li and J. R. Schmidt, *Chem. Rev.*, 2018, **118**, 3681–3721.
3 G. C. Sosso, J. Chen, S. J. Cox, M. Fitzner, P. Pedevilla, A. Zen and A. Michaelides, *Chem. Rev.*, 2016, **116**, 7078–7116.
4 N. Pienack and W. Bensch, *Angew. Chem., Int. Ed.*, 2011, **50**, 2014–2034.
5 J. F. Lutsko, *Sci. Adv.*, 2019, **5**, 1–8.
6 J. J. De Yoreo and N. A. J. M. Sommerdijk, *Nat. Rev. Mater.*, 2016, **1**, 16035.
7 N. D. Loh, S. Sen, M. Bosman, S. F. Tan, J. Zhong, C. A. Nijhuis, P. Král, P. Matsudaira and U. Mirsaidov, *Nat. Chem.*, 2017, **9**, 77–82.
8 M. H. Nielsen, S. Aloni and J. J. De Yoreo, *Science*, 2014, **345**, 1158–1162.
9 D. Li, M. H. Nielsen, J. R. I. Lee, C. Frandsen, J. F. Banfield and J. J. De Yoreo, *Science*, 2012, **336**, 1014–1018.
10 J. Xing, L. Schweighauser, S. Okada, K. Harano and E. Nakamura, *Nat. Commun.*, 2019, **10**, 3608.
11 H. Li, A. D. Chavez, H. Li, H. Li, W. R. Dichtel and J.-L. Bredas, *J. Am. Chem. Soc.*, 2017, **139**, 16310–16318.
12 D. Gebauer, M. Kellermeier, J. D. Gale, L. Bergström and H. Cölfen, *Chem. Soc. Rev.*, 2014, **43**, 2348–2371.
13 C. E. Hughes, P. A. Williams, B. M. Kariuki and K. D. M. Harris, *ChemPhysChem*, 2018, **19**, 3341–3345.
14 C. E. Hughes, P. A. Williams and K. D. M. Harris, *Angew. Chem., Int. Ed.*, 2014, **53**, 8939–8943.
15 B. Jagoda-Cwiklik, P. Slavíček, L. Cwiklik, D. Nolting, B. Winter and P. Jungwirth, *J. Phys. Chem. A*, 2008, **112**, 3499–3505.
16 D. Nolting, N. Ottosson, M. Faubel, I. V. Hertel and B. Winter, *J. Am. Chem. Soc.*, 2008, **130**, 8150–8151.
17 R. C. Burton, E. S. Ferrari, R. J. Davey, J. L. Finney and D. T. Bowron, *J. Phys. Chem. B*, 2009, **113**, 5967–5977.
18 Y. Hu, J. K. Liang, A. S. Myerson and L. S. Taylor, *Ind. Eng. Chem. Res.*, 2005, **44**, 1233–1240.
19 J. Cornel, C. Lindenberg and M. Mazzotti, *Ind. Eng. Chem. Res.*, 2008, **47**, 4870–4882.
20 A. Jorio, R. Saito, G. Dresselhaus and M. S. Dresselhaus, *Raman Spectroscopy in Graphene Related Systems*, Wiley, 2011.
21 M. S. Dresselhaus, G. Dresselhaus, R. Saito and A. Jorio, *Phys. Rep.*, 2005, **409**, 47–99.
22 G. Févotte, *Chem. Eng. Res. Des.*, 2007, **85**, 906–920.
23 Z. Liao and K. Wynne, *J. Am. Chem. Soc.*, 2022, **144**, 6727–6733.
24 O. Urquidi, J. Brazard, N. Lemessurier, L. Simine and T. B. M. Adachi, *Proc. Natl. Acad. Sci. U. S. A.*, 2022, **119**, 1–8.
25 Z. Liao and K. Wynne, *Proc. Natl. Acad. Sci. U. S. A.*, 2022, **119**, 2–3.
26 T. B. M. Adachi, J. Brazard and O. Urquidi, *Proc. Natl. Acad. Sci. U. S. A.*, 2022, **119**, e2207713119.
27 S. Khoshkhoo and J. Anwar, *J. Phys. D: Appl. Phys.*, 1993, **26**, B90–B93.
28 D. McManus, S. Vranic, F. Withers, V. Sanchez-Romaguera, M. Macucci, H. Yang, R. Sorrentino, K. Parvez, S.-K. Son, G. Iannaccone, K. Kostarelos, G. Fiori and C. Casiraghi, *Nat. Nanotechnol.*, 2017, **12**, 343–350.
29 J. Z. Wang, Z. H. Zheng, H. W. Li, W. T. S. Huck and H. Sirringhaus, *Nat. Mater.*, 2004, **3**, 171–176.
30 C. S. Handscomb, M. Kraft and A. E. Bayly, *Chem. Eng. Sci.*, 2009, **64**, 628–637.
31 E. V. Boldyreva, V. A. Drebushchak, T. N. Drebushchak, I. E. Paukov, Y. A. Kovalevskaya and E. S. Shutova, *J. Therm. Anal. Calorim.*, 2003, **73**, 409–418.
32 S. Sastry, *Nature*, 2005, **438**, 746–747.
33 S. V. Bykov, N. S. Myshakina and S. A. Asher, *J. Phys. Chem. B*, 2008, **112**, 5803–5812.
34 A. Alieva, M. Boyes, T. Vetter and C. Casiraghi, *CrystEngComm*, 2020, **22**, 7075–7081.

35 M. Boyes, A. Alieva, J. Tong, V. Nagyte, M. Melle-Franco, T. Vetter and C. Casiraghi, *ACS Nano*, 2020, **14**, 10394–10401.
36 P. C. Vioglio, P. Thureau, M. Juramy, F. Ziarelli, S. Viel, P. A. Williams, C. E. Hughes, K. D. M. Harris and G. Mollica, *J. Phys. Chem. Lett.*, 2019, **10**, 1505–1510.
37 S. K. Poornachary, J. V. Parambil, P. S. Chow, R. B. H. Tan and J. Y. Y. Heng, *Cryst. Growth Des.*, 2013, **13**, 1180–1186.
38 A. Y. Lee, I. S. Lee, S. S. Dette, J. Boerner and A. S. Myerson, *J. Am. Chem. Soc.*, 2005, **127**, 14982–14983.
39 A. B. M. Buanz and S. Gaisford, *Cryst. Growth Des.*, 2017, **17**, 1245–1250.
40 Y. Yu, K. Lin, X. Zhou, H. Wang, S. Liu and X. Ma, *J. Phys. Chem. C*, 2007, **111**, 8971–8978.
41 B. Sjöberg, S. Foley, B. Cardey and M. Enescu, *Spectrochim. Acta, Part A*, 2014, **128**, 300–311.
42 A. Y. Lee, I. S. Lee and A. S. Myerson, *Chem. Eng. Technol.*, 2006, **29**, 281–285.
43 N. V. Surovtsev, S. V. Adichtchev, V. K. Malinovsky, A. G. Ogienko, V. A. Drebushchak, A. Y. Manakov, A. I. Ancharov, A. S. Yunoshev and E. V. Boldyreva, *J. Chem. Phys.*, 2012, **137**, 065103.
44 J. Zaccaro, J. Matic, A. S. Myerson and B. A. Garetz, *Cryst. Growth Des.*, 2001, **1**, 5–8.